AGU ADVANCING EARTH AND SPACE SCIENCES

Geophysical Research Letters®

RESEARCH LETTER
10.1029/2023GL104369

Diapycnal Upwelling Over the Kyushu-Palau Ridge in the North Pacific Ocean

Xin Xiao[1,2], Chun Zhou[1,2,3], Qingxuan Yang[1,2,3], Zhiyou Jing[4], Zhiyu Liu[5], Dongliang Yuan[3,6,7,8], Zhenhua Xu[9], Wei Zhao[1,2,3], and Jiwei Tian[1,2,3]

[1]Frontier Science Center for Deep Ocean Multispheres and Earth System (FDOMES) and Physical Oceanography Laboratory, Sanya Oceanographic Institution, Ocean University of China, Qingdao/Sanya, China, [2]Key Laboratory of Ocean Observation and Information of Hainan Province, Sanya Oceanographic Institution, Ocean University of China, Sanya, China, [3]Laoshan Laboratory, Qingdao, China, [4]State Key Laboratory of Tropical Oceanography, South China Sea Institute of Oceanology, Chinese Academy of Sciences, Guangzhou, China, [5]State Key Laboratory of Marine Environmental Science, Department of Physical Oceanography, College of Ocean and Earth Sciences, Xiamen University, Xiamen, China, [6]Key Laboratory of Marine Science and Numerical Modeling, First Institute of Oceanography, Ministry of Natural Resources, Qingdao, China, [7]Shandong Key Laboratory of Marine Science and Numerical Modeling, Qingdao, China, [8]University of Chinese Academy of Sciences, Beijing, China, [9]CAS Key Laboratory of Ocean Circulation and Waves, Institute of Oceanology Chinese Academy of Sciences, Qingdao, China

Abstract A significant portion (~2.1 Sv, 1 Sv = 10^6 m^3 s^{-1}) of deep water penetrates into the Philippine Sea through the Yap-Mariana Junction, the sole passage of the Philippine Sea below 4,000 m, and is then upwelled into shallower layers, closing regional overturning circulation. Yet, the structure and variability of this diapycnal upwelling remain poorly understood. Here, we report on a fine-resolution hydrographic observation conducted at the most significant topographic feature in the Philippine Sea, the Kyushu-Palau Ridge (KPR). Enhanced mixing up to $O(10^{-2})$ m^2 s^{-1} near the KPR is manifested, indicating the presence of substantial upwelling herein. Besides, the ridge-related topography contributes more deep-water mass transformation than abyssal basins in the Philippine Sea. This study highlights the significant role of rough bathymetry features in generating diapycnal upwelling in the North Pacific.

Plain Language Summary In the North Pacific, a significant portion of deep water from the Antarctic enters the Philippine Sea below 4,000 m, where it is upwelled into shallower layers, closing regional overturning circulation. However, where the deep water gains buoyancy in the deep Philippine Sea required to upwell into shallower layers remains largely unknown, rendering our understanding of the western Pacific overturning circulation incomplete. To fill this gap, we conducted observations at two transects over the Kyushu-Palau Ridge (KPR), the most significant topographic feature in the Philippine Sea. Based on this observational program, we reveal the mixing structure down to the bottom across the KPR and estimate the deep water transformation in the deep Philippine Sea. This study illuminates the role of ridge-related topography in driving diapycnal upwelling in the deep ocean and improves our understanding of the deep circulation in the North Pacific Ocean.

Key Points:

- A three-dimensional distribution of diapycnal mixing over the Kyushu-Palau Ridge is presented
- The spatially variable of mixing across the Kyushu-Palau Ridge results in varying vertical velocities
- The Kyushu-Palau Ridge contributes more deep-water mass transformation than abyssal basins in the Philippine Sea

Supporting Information:

Supporting Information may be found in the online version of this article.

Correspondence to:

C. Zhou,
chunzhou@ouc.edu.cn

Citation:

Xiao, X., Zhou, C., Yang, Q., Jing, Z., Liu, Z., Yuan, D., et al. (2023). Diapycnal upwelling over the Kyushu-Palau ridge in the North Pacific Ocean. *Geophysical Research Letters*, *50*, e2023GL104369. https://doi.org/10.1029/2023GL104369

Received 4 MAY 2023
Accepted 24 AUG 2023

Author Contributions:

Conceptualization: Chun Zhou, Jiwei Tian
Formal analysis: Xin Xiao
Funding acquisition: Chun Zhou, Dongliang Yuan, Wei Zhao, Jiwei Tian
Project Administration: Chun Zhou, Zhiyou Jing, Wei Zhao, Jiwei Tian
Visualization: Xin Xiao
Writing – original draft: Xin Xiao, Chun Zhou
Writing – review & editing: Chun Zhou, Qingxuan Yang, Zhiyou Jing, Zhiyu Liu, Dongliang Yuan, Zhenhua Xu, Jiwei Tian

1. Introduction

The meridional overturning circulation is fed by dense waters sinking into the ocean abyss at high latitudes, redistributing heat and freshwater throughout the deep ocean (Talley, 2013). To maintain the overturning circulation, the dense deep water (below approximately 2,000 m) must upwell to the upper ocean via diabatic processes (Ferrari, 2014; Lumpkin & Speer, 2007; Marshall & Speer, 2012; Toole et al., 1994). The seminal studies of Munk (1966) and Munk and Wunsch (1998) highlighted the role of turbulent mixing in sustaining the deep-ocean stratification and overturning circulation, with an estimated average diapycnal diffusivity $\kappa \sim 10^{-4}$ m^2 s^{-1}. A cluster of in-situ measurements unprecedentedly revealed that enhanced turbulent mixing ($\kappa \sim 10$–100×10^{-4} m^2 s^{-1}) is concentrated at complicated topographic features, such as mid-ocean ridges (Garabato et al., 2004; Ledwell et al., 2000; Polzin et al., 1997; Thurnherr et al., 2005, 2019), canyons (Kunze et al., 2012; St. Laurent et al., 2001), seamounts (Carter et al., 2006; Kunze & Toole, 1997; Lueck & Mudge, 1997; Ye et al., 2022) and hydraulically controlled passages (Alford et al., 2013; Cusack et al., 2019; Mackinnon et al., 2008; Polzin et al., 1996; Tian et al., 2009; Voet et al., 2015).

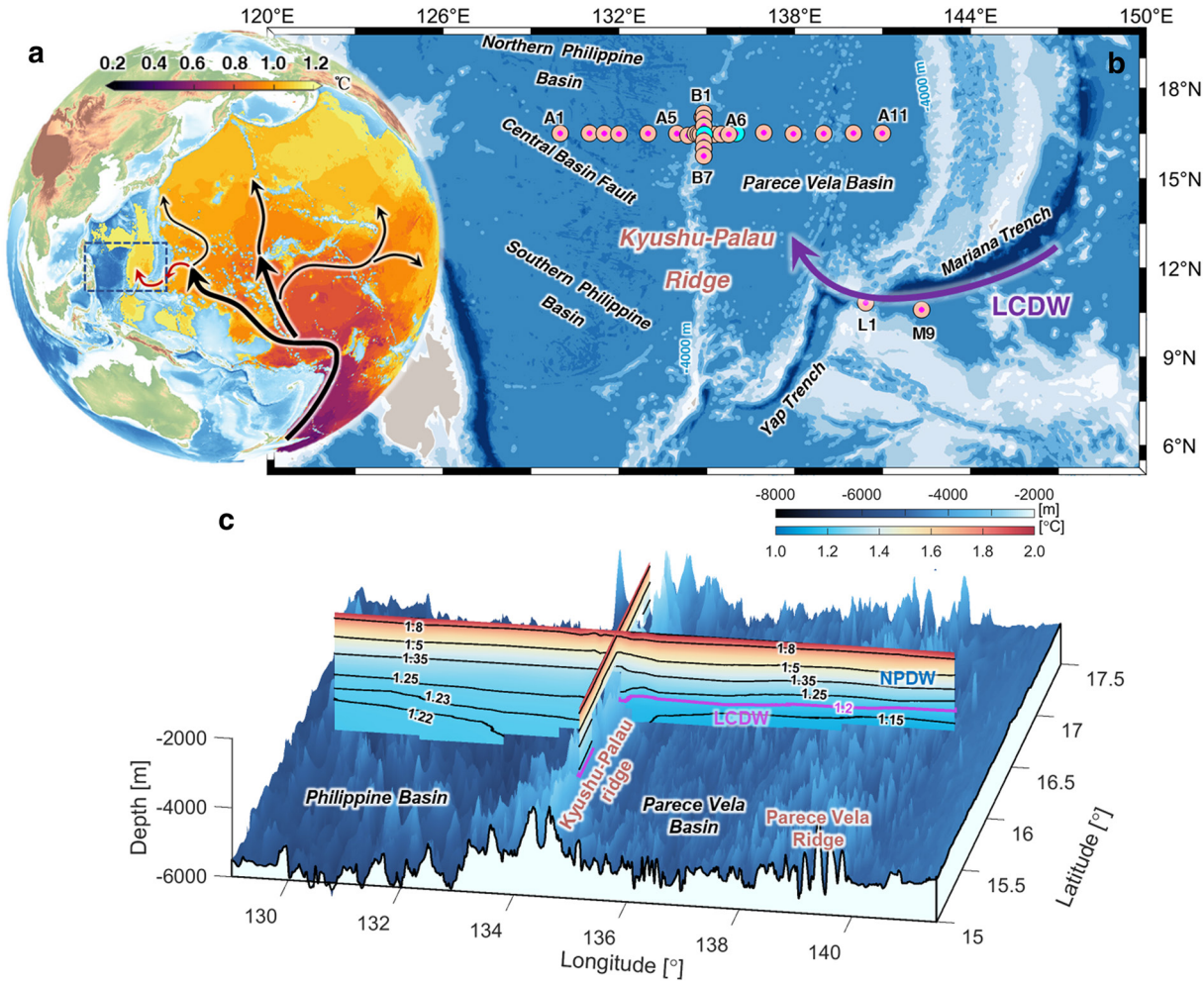

Figure 1. (a) Bathymetric map of the Pacific Ocean. Map shows the bottom potential temperature using data from the World Ocean Atlas. Schematic pathways of LCDW are indicated (Talley et al., 2011). (b) Hydrographic stations are indicated by pink double circles with two repeat-occupation stations in cyan. Schematic of LCDW's intrusion is indicated by thick arrows in magenta. (c) Spatial structure of potential temperature below 2,000 m.

The localized intense mixing impacts on the abyssal basin-scale circulation, supplies buoyancy flux, and links deep water to intermediate and upper layers to close the overturning circulation. For example, previous studies in the Brazil Basin indicated that following the intrusion of Antarctic Bottom Water through Vema Channel and Hunter Channel, more than 80% of the water transformation takes place near the Mid-Atlantic Ridge rather than on the abyssal plain (Thurnherr et al., 2005, 2019), which is associated with the intense mixing observed over the western flank of the Mid-Atlantic Ridge (Polzin et al., 1997). Theoretical and numerical studies further addressed the regulation dynamics of bottom-enhanced diapycnal mixing on deep-ocean water-mass transformation and upwelling occurring near the mid-ocean ridge (e.g., Drake et al., 2020; Ferrari, 2014).

In the North Pacific, the Philippine Sea manifests similar features to that of the Brazil Basin. The deep Philippine Sea below 4,000 m is linked to the surrounding waters by the only choke point, Yap-Mariana Junction (YMJ). Inside the Philippine Sea, the deep basin is divided by the north-south oriented Kyushu-Palau Ridge (KPR) into several sub-basins, that is, the Philippine Basin (PB) to the west, and the Parece Vela Basin (PVB) and the Shikoku Basin to the east. The Lower Circumpolar Deep Water (LCDW), which originates from the Southern Ocean, flows along topographically-guided pathways to the North Pacific Ocean (Figure 1a). A significant portion (~2.1 Sv) of LCDW enroutes the YMJ and supplies water masses to the deep Philippine Sea (Siedler et al., 2004; Wang et al., 2021a, 2021b; Zhou et al., 2022). Previous studies indicate a preliminary picture of horizontal pathways of deep waters in the Philippine Sea based on inverse modeling (Kaneko et al., 2001; Tian et al., 2021), reanalysis data (Zhai & Gu, 2020) and direct observations (Chaen et al., 1993; Komaki & Nagano, 2018; Uehara

& Taira, 1990; Yoshioka et al., 1988; Zhai et al., 2014; Zhou et al., 2018). The LCDW is expected to upwell somewhere, regulating the overturning circulation and biogeochemical properties in the Philippine Sea. However, where the LCDW gains buoyancy required to upwell into shallower layers remains largely unknown, rendering our understanding of the western Pacific overturning circulation incomplete.

As a prominent bathymetric high in the middle Philippine Sea stretching over 2,600 km with steep and rugged bottom topography as well as energetic internal tides (Wang et al., 2018), the KPR acts as a potential hotspot for deep water upwelling, like the Mid-Atlantic Ridge. To better characterize the structure and evolution of the deep water in the deep Philippine Sea, hydrographic observations were conducted over the KPR (Figure 1b) to investigate the water mass characteristics and the upwelling of deep water in the Philippine Sea.

2. Materials and Methods

2.1. Data

From 23 September to 22 October 2021, observations at 31 stations (Figure 1b, Table S1 in Supporting Information S1) were conducted using Seabird 911 Plus Conductivity-Temperature-Depth (CTD). One transect cuts across the KPR with approximately 1° spacing in the PB and PVB and a minimum of 2 km near the KPR, and the other transect runs basically along the KPR with station spacing of 0.25°. A single CTD profile was taken at most of the stations except two stations located near the KPR, that is, A6 and B4, which were repeated to resolve tidal variability (9 profiles at each station). Two stations were located at the Mariana Trench (MT), measuring upstream properties of the LCDW. At all the stations except station A6, nearly full-depth CTD profiles were conducted down to an average of 50 m height above the bottom. With the pre-cruise calibrations, the accuracies of the CTD sensors are <0.001 psu for salinity and ±0.001°C for temperature. The CTD data were quality controlled for further analysis.

Temperature and salinity data used outside the observation area are from the World Ocean Atlas 2013 (Locarnini et al., 2013; Zweng et al., 2013). Barotropic tidal currents were extracted from TPXO9 with 1/30° resolution (Egbert & Erofeeva, 2002). CTD profiles from World Ocean Database (WOD) are used to evaluate the upwelling transport in adjacent regions (Boyer et al., 2018). Fine-resolution topography at the two transects was measured using a multi-beam echo sounder system. Additionally, the Shuttle Radar Topography Mission data set at 15-arc-second resolution (SRTM15+) is used. The SRTM15+ is significantly enriched by small-scale topographic features (Tozer et al., 2019).

2.2. Methods

2.2.1. Gregg–Henyey–Polzin Parameterization

Turbulent kinetic energy dissipation rate ε is inferred using the widely employed Gregg-Henyey-Polzin (GHP) parameterization based on internal wave–wave interaction (Gregg et al., 2003), which has provided reasonable estimation of ε in mixing hotspots in the Western Pacific (Hibiya et al., 2012). The specific strain-based form of the parameterization is

$$\varepsilon = \varepsilon_0 \frac{N^2}{N_0^2} \frac{\left\langle \xi_z^2 \right\rangle^2}{{}_{GM}\left\langle \xi_z^2 \right\rangle^2} h(R_\omega) j\left(\frac{f}{N}\right) \tag{1}$$

where $\varepsilon_0 = 6.73 \times 10^{-10}$ W kg^{-1}, and f and N are the Coriolis and buoyancy frequencies, respectively. The term R_ω is defined as $R_\omega = \left\langle V_z^2 \right\rangle / \left\langle \xi_z^2 \right\rangle$, where $\left\langle V_z^2 \right\rangle$ and $\left\langle \xi_z^2 \right\rangle$ represent the fine-scale internal wave shear and strain variance. ${}_{GM}\left\langle \xi_z^2 \right\rangle$ is the strain variance estimated from the Garret and Munk spectrum (Garrett & Munk, 1972, 1975). Strain-based dissipation rates with $R_\omega = 7$ agree to within a factor of 2 with shear-and-strain dissipation rates from GHP (Kunze et al., 2006). As a result, dissipation rates are estimated from CTD strain and a constant of R_ω. Stain profiles with a resolution of 10 m were divided into half-overlapping 320-m-long segments starting from the bottom. The strain variance was obtained by integrating strain spectra from a variable minimum vertical wavelength (50–90 m) to a maximum (320 m) to avoid instrument noise at higher wavenumbers (Tian et al., 2009):

$$\left\langle \xi_z^2 \right\rangle = \int_{k_{\min}}^{k_{\max}} S_{\xi_z}(k_z) dk_z \tag{2}$$

2.2.2. Thorpe-Scale Method

The ε is also estimated using the Thorpe scale method, $\varepsilon = 0.64 L_T^2 N^3$ (Thorpe, 1977). To estimate the diapycnal diffusivity κ from the GHP and Thorpe-scale method inferred ε, the Osborn (1980) formula with $\Gamma = 0.2$ is used, which is

$$\kappa = \Gamma \frac{\varepsilon}{N^2} \tag{3}$$

A drawback of the Thorpe-scale method is that overturns could not be easily detected if there exists a strong or too weak stratification. Therefore, our analysis mainly relies on the GHP method in this study and we use the Thorpe-scale method for comparison. The diffusivity estimates based on the GHP and Thorpe-scale method yield reasonable consistency (Figure S1 in Supporting Information S1).

2.2.3. Internal Tide

The vertical displacement $\eta\left(\langle z(\sigma_\theta)\rangle_t, t\right)$ is computed through $\eta\left(\langle z(\sigma_\theta)\rangle_t, t\right) = z(\sigma_\theta, t) - \langle z(\sigma_\theta)\rangle_t$ (Desaubies & Gregg, 1981). Here $z(\sigma_\theta, t)$ is the potential density measurement, and $\langle z(\sigma_\theta)\rangle_t$ is the time-averaged depth of $z(\sigma_\theta, t)$. The depth-integrated available potential energy (APE) is calculated by:

$$\mathrm{APE} = \left\langle \frac{1}{2} \int_{-H}^{0} N^2(z,t)\eta(z,t)dz \right\rangle \tag{4}$$

The baroclinic modes for vertical displacement $\Phi_n(z)$ are defined as the solutions of the eigenvalue problem (Gill, 1982)

$$\frac{d^2\Phi_n}{dz^2} + \frac{N^2(z)}{c_n^2}\Phi_n(z) = 0 \tag{5}$$

with boundary conditions $\Phi_n(0) = \Phi_n(-H) = 0$, where subscript n is the baroclinic mode number and c_n is the eigenspeed, defined as

$$c_n = \frac{1}{n\pi} \int_{-H}^{0} N(z)dz \tag{6}$$

The corresponding modes for pressure and horizontal velocity $\prod_n(z)$ are defined as

$$\prod_n(z) = \rho_0 c_n^2 \frac{d\Phi_n(z)}{dz} \tag{7}$$

To project vertical displacement onto the first ten modes ($n = 1, 2, 3, \ldots, 10$), the least squares fit method is used (Nash et al., 2006). The equivalent mode number is toward the internal tide, which is determined by the modal dispersion relation given by

$$k_j = \frac{j\pi}{H}\left(\frac{\omega^2 - f^2}{\overline{N}^2 - \omega^2}\right)^{1/2} \tag{8}$$

where j is the mode number; k_j is the corresponding horizontal wavenumber, H and f are the mean water depth and Coriolis frequency in the selected region, respectively. The ω is the tidal frequency.

2.2.4. Diapycnal Velocity

Diapycnal velocity w_* can be calculated from McDougall (1984) derived equation. If the isopycnal diffusivity term and double diffusion can be ignored, the equation is written as

$$w_* = \frac{1}{N^2}\frac{\partial}{\partial z}(\Gamma\varepsilon) + \frac{g}{N^2}\left[-\frac{\partial\alpha}{\partial\theta}\kappa\theta_z^2 - \frac{\partial\alpha}{\partial p}\kappa\theta_z p_z\right] \tag{9}$$

where α is the thermal expansion coefficient and p is pressure. The subscript z denotes derivative with respect to depth. Here, logarithmic fits to dissipation rate profiles are used to calculate w_*.

3. Results

3.1. Three-Dimensional Distribution of Water Properties and Mixing in the Deep Philippine Sea

Sections of potential temperature (θ, Figure 1c), potential density (σ_2, Figure S2 in Supporting Information S1) along and across the KPR exhibit the distribution of water properties in the deep Philippine Sea. The 1.2°C isotherm or 36.04 kg m^{-3} isopycnal at depth of ~4,000 m demonstrate the intrusion of cold, saline and dense LCDW (θ < 1.2°C) from the YMJ. Due to the topographic constraint of the KPR, no LCDW is identified on the western half of the section. This is consistent with previous studies (Tian et al., 2021; Wang et al., 2023), which suggests that the LCDW penetrates through the gaps of the KPR to the north and constrain at the Northern Philippine Basin. Therefore, notable difference of water mass properties is manifested between the deep water to the east and west of the KPR, resulting in weaker stratification in the PB. Nevertheless, the isotherms (e.g., 1.15°C, 1.2°C, 1.22°C, and 1.23°C isotherms) below 4,000 m on both sides of the KPR slope downward while approaching the KPR, indicating the existence of vigorous turbulent mixing and water mass transport along the slope of the KPR.

Water masses above 3,000 m (Figure 2a) are discernible evidently but they were outside the scope of present study focusing on deep water. The deep water below 3,500 m undergoes a significant increase in temperature and a decrease in density and salinity as it transitions from the MT to the PVB (Figure 2b). Although there are several gaps, where deep water exchanged between the PB and PVB (Wang et al., 2023), at the KPR below 3,800 m, the deep water in the PB is distinctly warmer and lighter than that in the PVB. Additionally, it is worth noting that the deep water exhibits a remarkable warming and lightening trend from the PB eastward to the KPR and from the PVB westward to the KPR (Figures 2c and 2d). This trend is associated with the sloping isolines and is likely influenced by the mixing that occurs near the KPR.

Based on the fine-scale parameterization, the three-dimensional structure of diapycnal mixing over the KPR is illustrated in Figure 3. Vertically, a substantial bottom intensified structure, resembling previous findings of Kunze et al. (2006), is also suggested. Horizontally, inhomogeneous spatial distribution of turbulent dissipation and mixing is manifested, which is tightly related to the rough KPR. There is a remarkable enhancement in dissipation ($O[10^{-7}\ m^2\ s^{-3}]$) and diffusivity ($O[10^{-3}\ m^2\ s^{-1}]$) near the KPR below 2,000 m. These elevated diffusivity values near the KPR are comparable to those observed in other basins (Polzin et al., 1997; Sloyan, 2006). Eight profiles in meridional and eight densely-spaced profiles in zonal represent profiles near the KPR, while the remaining 13 profiles in the PB and PVB are on behalf of profiles outside KPR. Averaged profiles of diffusivity and dissipation near the KPR highlight the enhanced mixing near the KPR, with values approximately one order of magnitude larger than the relatively flat PB and PVB, yet there is insignificant difference above 1,500 m (Figures 3c and 3f). This enhanced mixing coincides with sloping isotherms and isopycnals in the vicinity of the KPR. Kunze et al. (2006) revealed that sharp pycnoclines in the background stratification to contaminate estimates of internal wave strain variance, particularly affecting strain-only estimates. Nevertheless, this contamination is less pronounced in our study, as we specifically focus on processes below 2,000 m, which are considerably distant from the pycnoclines. The uncertainties of GHP method might affect the mixing pattern overall in the deep ocean but the enhanced mixing near the KPR is still reliable.

The breaking of internal tides generated over rough topography has been suggested to be the main contributor to the intensified turbulent mixing in deep ocean (Bell, 1975; Garrett & Kunze, 2007; Vic et al., 2019). Tidal energy budget analysis at Mid-Atlantic Ridge highlighted the significance of the generation of the high-mode internal tides (Vic et al., 2018), which are more prone to near-field dissipation (St. Laurent & Nash, 2004; Vic et al., 2018). Utilizing data from two repeat stations, one located near the top of the KPR (B4) and the other in the relatively flat PVB (A6), the APE of tidal generation is evaluated. Profiles at B4 extended down to the bottom of ~3,300 m, whereas those at A6 extended down to ~2,000 m. When comparing results of the generated internal tides above the upper 2,000 m with full-depth profiles at B4, the differences were found to be small. Therefore, we utilize the upper 2,000 m profiles from A6 for further analysis. The displacement η is projected qualitatively onto 10 modes. The generated APE of internal tides varies at the two stations (Figure 4a). Mode-1 APE of A6 accounts for 58% of the energy density of modes 1–10, while mode-1 APE of B4 accounts for only 34% (37% using upper 2,000 m profiles). This suggests that more high-mode internal tides, presumably locally generated exist near the KPR compared to inside the deep basin, and likely dissipated locally to furnish mixing (Vic et al., 2018). The wavelet spectrum of multibeam bathymetric data of zonal section is distinctly different at the two stations (Figure S3 in Supporting Information S1). At B4, the spectrum density exhibits a high level at both small and

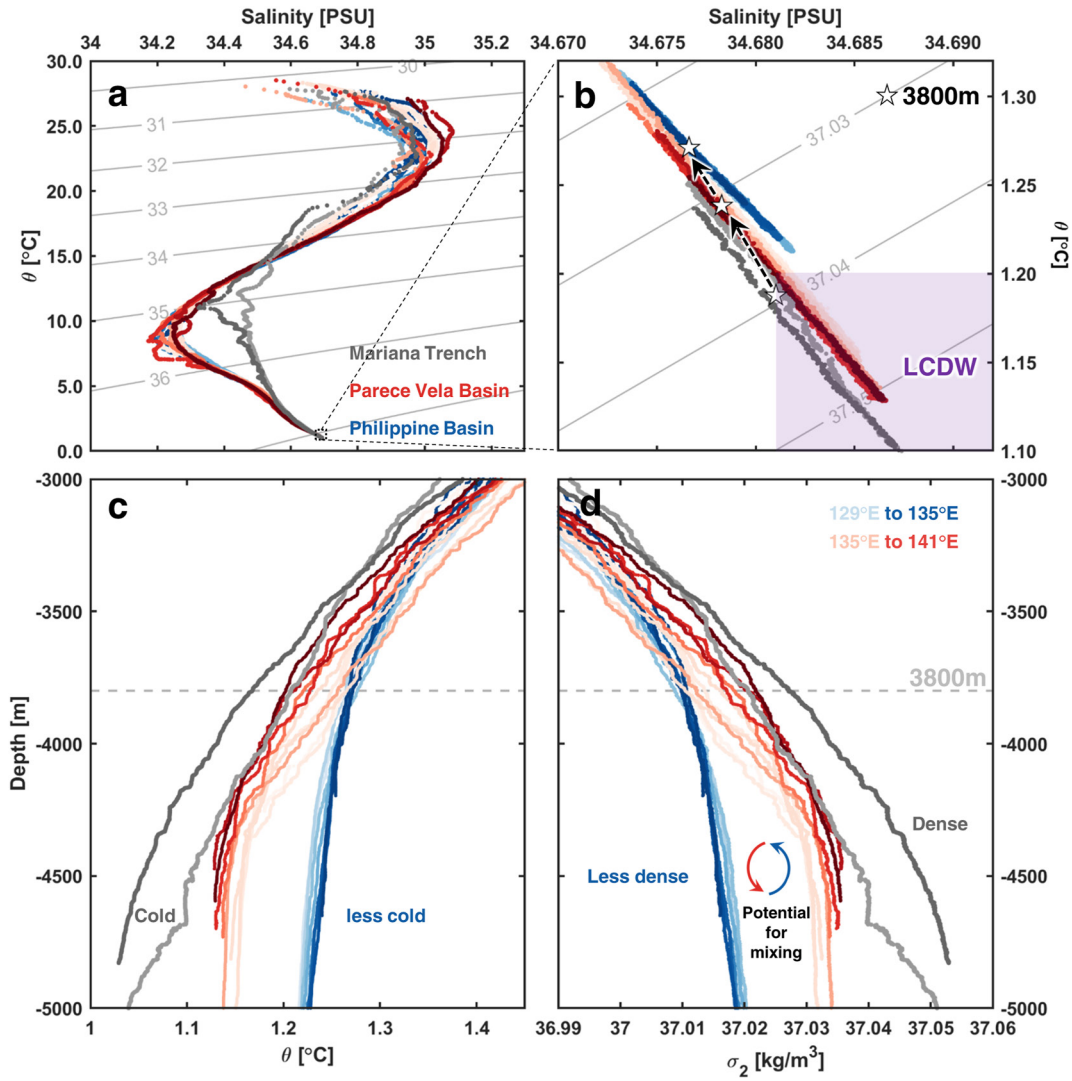

Figure 2. (a) Relation of potential temperature versus salinity (with contours overlain) along zonal section in the Philippine Basin (PB, in blue), Parece Vela Basin (PVB, in red) and two stations at Mariana Trench (MT, in gray). The gray contours with numbers stand for the potential density. The darker the color, the further east the location is. Panel (b) same as (a) except for depth below 3,500 m. White stars indicates 3,800 m in the PB, PVB and MT, respectively. (c) Potential temperature and (d) potential density profiles of along zonal section below 3,000 m.

large wavelengths (50–200 km). While at A6, the spectrum peaks at wavelengths larger than 120 km. The equivalent mode numbers for the diurnal tide imply that internal tides with high vertical modes are prevalent near the KPR, which is consistent with the results of the generated APE (Figure 4a). Due to limitation of velocity data, we could not obtain a reliable analysis of baroclinic horizontal kinetic energy (HKE). But, for a single wave, the ratio between HKE and APE is generally following HKE/APE = $(\omega^2 + f^2)/(\omega^2 - f^2)$, where ω is the tidal frequency and f is the inertial frequency. As a result, the analysis of the energy budget of internal tides is reasonable.

3.2. Upwelling in the Deep Philippine Sea

After intruding into the Philippine Sea through the YMJ, LCDW has to upwell to upper layers via diabatic processes. Given that the YMJ is the only deep passage below 4,000 m and the area of 3.9×10^6 km^2 at 4,000 m of the Philippine Sea (see topography in Figure 4c), LCDW transport of 2.1 ± 0.4 Sv (Zhou et al., 2022) would be accompanied by an averaged upwelling rate of $(0.54 \pm 0.10) \times 10^{-6}$ ms^{-1}, nearly four times larger than Munk's assumption for the global ocean average ($w_* = 0.14 \times 10^{-6}$ ms^{-1}, Munk, 1966). It is of interest to understand where the deep water upwells to the upper layers of the Philippine Sea.

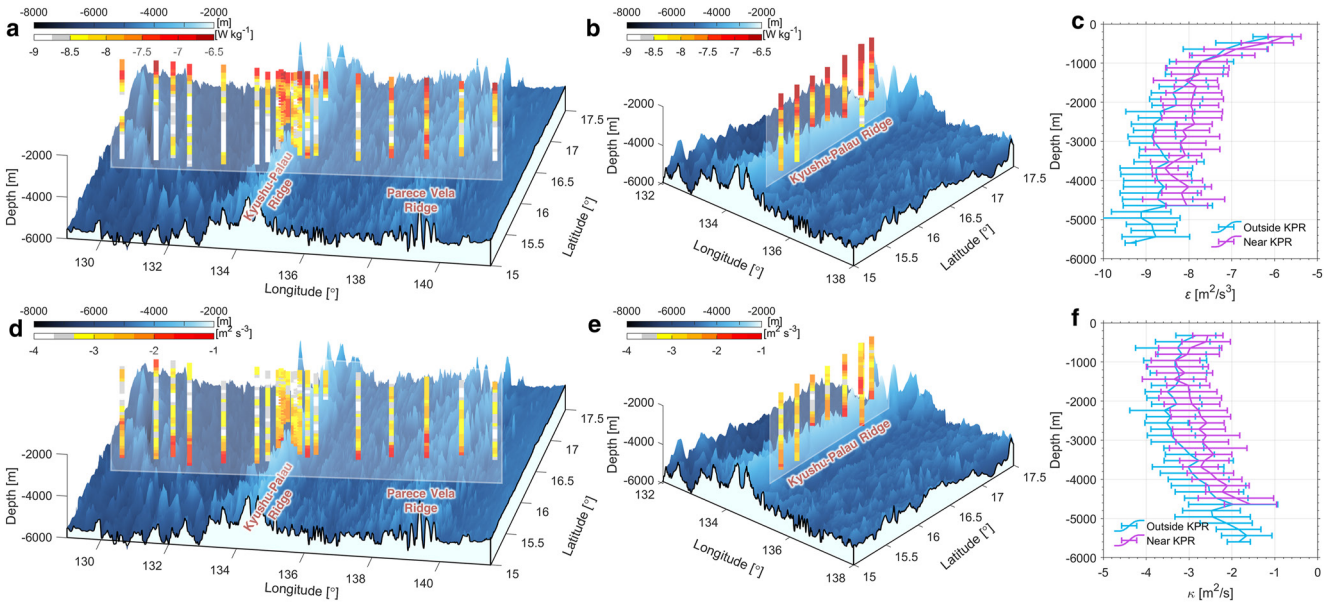

Figure 3. Spatial structure of turbulent dissipation (a) across the Kyushu-Palau Ridge (KPR) and (b) along the KPR and (c) average profiles of dissipation rate near (in magenta) and outside (in cyan) the KPR with errorbars showing the standard deviation. (d)–(f) are the same as (a)–(c) but for the diffusivity. Logarithmic scales are used for the dissipation and diffusivity.

Diapycnal velocity w_* can be calculated from Equation 9 (e.g., Du et al., 2017; Groeskamp et al., 2016). Note that this w_* does not consider the upward components driven by wind stress curl or convergence and divergence. The errors (or 95% confidence interval) of derived w_* are given by the averaged profiles of N^2 and ε. A persistent upwelling is indicated with magnitudes on the order of 10^{-6} ms^{-1} below 2,000 m (Figure 4b). This upwelling weakens as the depth becomes shallower, with the maximum upwelling of approximately $(4.18 \pm 1.25) \times 10^{-6}$ ms^{-1} near the KPR and $(3.50 \pm 1.11) \times 10^{-6}$ ms^{-1} outside the KPR, both of which are found near the bottom. The estimated upwelling rate of $(0.54 \pm 0.10) \times 10^{-6}$ ms^{-1} calculated using LCDW transport is

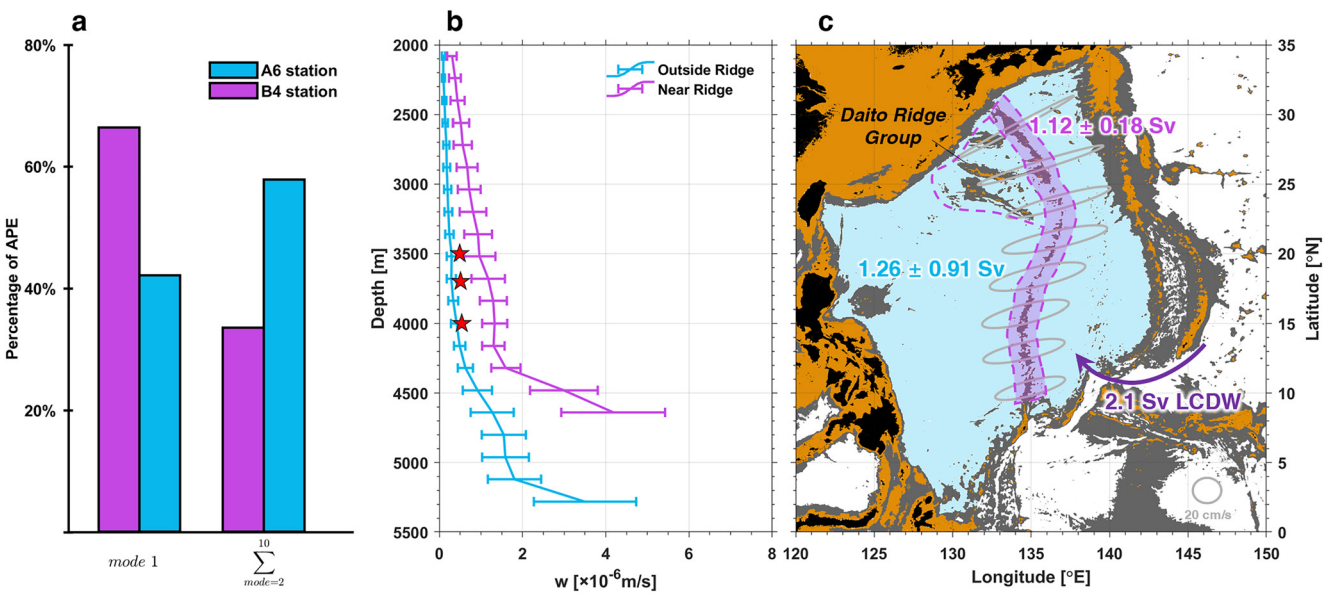

Figure 4. (a) The percentage of mode 1 and modes 2–10 of the Available Potential Energy (APE) at B4 and A6. (b) Vertical velocity profiles below 2,000 m. Errorbars indicate the 95% confidence interval of the mean value. The red stars are the average vertical velocity at 3,500 m, 3,700 m, and 4,000 m, based on the transport at the Yap-Mariana Junction. (c) Estimates of upwelling transport in the basin and near the Kyushu-Palau Ridge (KPR). The dotted line stands for the area of ridge-related topography, with the KPR filled in magenta. Tidal ellipses are indicated in gray along the KPR.

basically between the strong upwelling ($[1.33 \pm 0.30] \times 10^{-6}$ ms^{-1}) near the KPR and relatively weak upwelling ($[0.41 \pm 0.30] \times 10^{-6}$ ms^{-1}) outside the KPR at 4,000 m. This suggests that most of the deep water would upwell near the KPR, while much weaker upwelling take place inside the deep basin of the Philippine Sea. The results at 3,500 and 3,700 m are consistent with those at 4,000 m (Figure 4b).

Mixing in the KPR is modulated by locally generated internal tides. The generated internal tides' energy is proportional to the buoyancy frequency N, the wavenumber and the amplitude that characterizes the bathymetry (k, h) and the barotropic tidal velocity $\vec{u}$ (Jayne & St. Laurent, 2001). In attempt to estimate the water mass upwelling, we conducted comprehensive analysis of the bathymetries, stratification and barotropic tides along the KPR. First, we calculated the mean spectra using SRTM15+ data within two regions: one near the KPR, which spans about 200 km in width with the shallowest point at the center, and the other outside the KPR, which is about 150–200 km away from the KPR, according to the location of station B4 and A6, respectively. The results suggested similar topographic features along the entire KPR in spectral space (Figure S3 in Supporting Information S1). Subsequently, we obtained the average stratification N^2 below 2,000 m near the KPR. The magnitude of the averaged N^2 along the KPR is within a factor of two (Figure S3 in Supporting Information S1). Finally, we analyzed the barotropic tides along the KPR from TPXO9, which indicates that the major axes of the tidal ellipse are zonally dominated and almost identical to the KPR (Figure 4c). Consequently, it can be inferred that the generation of internal tides is similar throughout the entire KPR based on these findings. Here, the ridge-related topography in the northern KPR, that is, the Daito Ridge Group (DRG), is also considered in these aspects. Besides, the analysis based on WOD data suggests that upwelling volume certainly should not be neglected at the Daito Ridge Group (Table S2 in Supporting Information S1).

The Philippine Sea at 4,000 m can be divided into two major areas, that is, the area near the ridge-related topography (the KPR and the DRG) and the relatively flat deep basin. The former covers approximately 0.84×10^6 km^2 (accounting for 21%), while the latter covers 3.06×10^6 km^2 (accounting for 79%). Using the average vertical velocity estimates near and outside the KPR at 4,000 m above, the upwelling volume is estimated to be 1.12 ± 0.18 Sv and 1.26 ± 0.91 Sv near and outside the KPR at 4,000 m, respectively. The estimate of 2.38 ± 0.93 Sv in total is close to the observed volume transport of around 2.1 Sv through the YMJ below 4,000 m (Zhou et al., 2022) and is similar to the result (2.42 ± 0.67 Sv) when taking other potential mixing hotspots into account (Figure S5 in Supporting Information S1), which strengthens our speculation. This estimate presents a primary pattern for mixing-induced upwelling in the deep Philippine Sea. The ridge-related topography accounts for only 21% of the deep Philippine Sea at 4,000 m, but contributes 47% of deep water upwelling. A similar pattern was revealed in the Brazil Basin, where 15% of the upper interfacial area of deep water lies at the mid-ocean ridge, yet approximately one-half of the diapycnal buoyancy fluxes take place there (Thurnherr et al., 2005, 2019).

4. Discussion

A significant portion of deep water enters the Philippine Sea below 4,000 m, through the only deep passage namely YMJ. We reveal that the KPR is an upwelling hotspot due to enhanced mixing. The APE budget suggests that the internal tides generated in the KPR are more likely contribute to the enhanced mixing. However, part of the generated lower-mode internal tides in the Mariana Arc and Luzon Strait could propagate to the KPR and the refraction and interference effects of these internal tides could affect mixing near the KPR (Chen et al., 2021; Wang et al., 2021a, 2021b; Xu et al., 2021; Zhao et al., 2016, 2021). Besides, other energetic dynamic processes were revealed in the deep Philippine Sea, such as bottom current across the KPR (Wang et al., 2023) and deep eddies in the PB (Ma et al., 2023). The energy from these geostrophic flows into lee waves can break and sustain enhanced turbulent mixing (e.g., Nikurashin & Ferrari, 2011; Voet et al., 2020). Further confirmation of the role of low-mode internal tides and lee waves is required in the future.

The diapycnal upwelling near and outside the KPR are assessed at 4,000 m, highlighting the important role of ridge-related topography played in water mass transformation. The estimated 2.38 ± 0.93 Sv upwelling transport is comparable with the observed volume transport at YMJ (2.1 Sv). There is not distinct bias (2.42 ± 0.67 Sv) when taking other mixing hotspots into consideration. The upwelling of the deep water in the Pacific is related to the variability of the Indonesian Throughflow and the warm pool, regulating the regional climate system (Feng et al., 2017; Holzer et al., 2021; Hu et al., 2015; Sen Gupta et al., 2016; Talley, 2013). Therefore, our study urges observational, theoretical and modeling efforts toward incorporating rough topography effects on Pacific overturning circulation.

Data Availability Statement

The global bathymetry and topography at 15 arcseconds (SRTM15+) data are downloaded from https://topex.ucsd.edu/www_html/srtm15_plus.html. The WOA hydraulic data are from https://www.nodc.noaa.gov/OC5/woa13/. The WOD data can be accessed at https://www.ncei.noaa.gov/products/world-ocean-database. The barotropic tides (TPXO9) are from https://www.tpxo.net/. The hydrographic observations are available at the Zendo repository (https://doi.org/10.5281/zenodo.7895316).

Acknowledgments

This study was supported by the National Natural Science Foundation of China (Grant 42076027, 92258301, 91858205, 41720104008, 91858204) and the "Taishan" Talents program (tsqn202306094). D. Yuan is also supported by National Key R&D Program of China (2020YFA0608800), Laoshan Laboratory (No. 2022LSL010304-4), the Strategic Priority Research Program of the Chinese Academy of Sciences (XDB42000000), the "Taishan Scholar Project" of the Shandong province and the "Kunpeng Outstanding Scholar Program" of the FIO/MNR of China. The authors thank the cruise NORC2021-582 supported by NSFC Shiptime Sharing Project (Grant 42049582) and thank the crew of the *R/V Dongfanghong 3*.

References

Alford, M. H., Girton, J. B., Voet, G., Carter, G. S., Mickett, J. B., & Klymak, J. M. (2013). Turbulent mixing and hydraulic control of abyssal water in the Samoan Passage. *Geophysical Research Letters*, *40*(17), 4668–4674. https://doi.org/10.1002/grl.50684

Bell, T. H. (1975). Topographically generated internal waves in the open ocean. *Journal of Geophysical Research*, *80*(3), 320–327. https://doi.org/10.1029/jc080i003p00320

Boyer, T. P., Baranova, O. K., Coleman, C., Garcia, H. E., Grodsky, A., Locarnini, R. A., et al. (2018). World ocean database 2018. In A. V. Mishonov & Technical (Eds.), *NOAA Atlas NESDIS 87*. Retrieved from https://www.ncei.noaa.gov/sites/default/files/2020-04/wod_intro_0.pdf

Carter, G. S., Gregg, M. C., & Merrifield, M. A. (2006). Flow and mixing around a small seamount on Kaena Ridge, Hawaii. *Journal of Physical Oceanography*, *36*(6), 1036–1052. https://doi.org/10.1175/jpo2924.1

Chaen, M., Fukasawa, M., Maeda, A., Sakurai, M., & Takematsu, M. (1993). Abyssal boundary current along the Northwestern perimeter of the Philippine Basin. *Elsevier Oceanography Series*, *59*, 51–67. https://doi.org/10.1016/S0422-9894(08)71317-5

Chen, Q. A., Yu, L., Yang, Q., Vetter, P. A., Xu, H., Xie, Q., et al. (2021). Model simulation of M2 internal tide at the Mariana double Ridges. *Journal of Marine Science and Engineering*, *9*(6), 592. https://doi.org/10.3390/jmse9060592

Cusack, J. M., Voet, G., Alford, M. H., Girton, J. B., Carter, G. S., Pratt, L. J., et al. (2019). Persistent turbulence in the Samoan passage. *Journal of Physical Oceanography*, *49*(12), 3179–3197. https://doi.org/10.1175/jpo-d-19-0116.1

Desaubies, Y., & Gregg, M. (1981). Reversible and irreversible fine structure. *Journal of Physical Oceanography*, *11*(4), 541–556. https://doi.org/10.1175/1520-0485(1981)011<0541:RAIF>2.0.CO;2

Drake, H. F., Ruan, X., & Ferrari, R. (2020). Diapycnal displacement, diffusion, and distortion of tracers in the ocean. *Journal of Physical Oceanography*, *52*(12), 3221–3240. https://doi.org/10.1175/jpo-d-22-0010.1

Du, C., Liu, Z., Kao, S. J., & Dai, M. (2017). Diapycnal fluxes of nutrients in an oligotrophic oceanic regime: The South China Sea. *Geophysical Research Letters*, *44*(22), 11510–11518. https://doi.org/10.1002/2017gl074921

Egbert, G. D., & Erofeeva, S. Y. (2002). Efficient inverse modeling of barotropic ocean tides. *Journal of Atmospheric and Oceanic Technology*, *19*(2), 183–204. https://doi.org/10.1175/1520-0426(2002)019<0183:EIMOBO>2.0.CO;2

Feng, M., Zhang, X., Sloyan, B., & Chamberlain, M. (2017). Contribution of the deep ocean to the centennial changes of the Indonesian Throughflow. *Geophysical Research Letters*, *44*(6), 2859–2867. https://doi.org/10.1002/2017gl072577

Ferrari, R. (2014). What goes down must come up. *Nature*, *513*(7517), 179–180. https://doi.org/10.1038/513179a

Garabato, A. C. N., Polzin, K. L., King, B. A., Heywood, K. J., & Martin, V. (2004). Widespread intense turbulent mixing in the Southern Ocean. *Science*, *303*(5655), 210–213. https://doi.org/10.1126/science.109092

Garrett, C., & Kunze, E. (2007). Internal tide generation in the deep ocean. *Annual Review of Fluid Mechanics*, *39*(1), 57–87. https://doi.org/10.1146/annurev.fluid.39.050905.110227

Garrett, C., & Munk, W. (1972). Space-time scales of internal waves. *Geophysical Fluid Dynamics*, *3*(3), 225–264. https://doi.org/10.1080/03091927208236082

Garrett, C., & Munk, W. (1975). Space-time scales of internal waves: A progress report. *Journal of Geophysical Research*, *80*(3), 291–297. https://doi.org/10.1029/jc080i003p00291

Gill, A. E. (1982). *Atmosphere-ocean dynamics*. Academic press. https://doi.org/10.1016/s0074-6142(08)x6002-4

Gregg, M. C., Sanford, T. B., & Winkel, D. P. (2003). Reduced mixing from the breaking of internal waves in equatorial waters. *Nature*, *422*(6931), 513–515. https://doi.org/10.1038/nature01507

Groeskamp, S., Abernathey, R. P., & Klocker, A. (2016). Water mass transformation by cabbeling and thermobaricity. *Geophysical Research Letters*, *43*(20), 10835–10845. https://doi.org/10.1002/2016gl070860

Hibiya, T., Furuichi, N., & Robertson, R. (2012). Assessment of fine-scale parameterizations of turbulent dissipation rates near mixing hotspots in the deep ocean. *Geophysical Research Letters*, *39*(24), L24601. https://doi.org/10.1029/2012gl054068

Holzer, M., DeVries, T., & de Lavergne, C. (2021). Diffusion controls the ventilation of a Pacific Shadow Zone above abyssal overturning. *Nature Communications*, *12*(1), 4348. https://doi.org/10.1038/s41467-021-24648-x

Hu, D., Wu, L., Cai, W., Gupta, A. S., Ganachaud, A., Qiu, B., et al. (2015). Pacific western boundary currents and their roles in climate. *Nature*, *522*(7556), 299–308. https://doi.org/10.1038/nature14504

Jayne, S. R., & St. Laurent, L. C. (2001). Parameterizing tidal dissipation over rough topography. *Geophysical Research Letters*, *28*(5), 811–814. https://doi.org/10.1029/2000GL012044

Kaneko, I., Takatsuki, Y., & Kamiya, H. (2001). Circulation of intermediate and deep waters in the Philippine Sea. *Journal of Oceanography*, *57*(4), 397–420. https://doi.org/10.1023/A:1021565031846

Komaki, K., & Nagano, A. (2018). Monitoring the deep western boundary current in the western North Pacific by echo intensity measured with lowered acoustic Doppler current profiler. *Marine Geophysical Researches*, *40*(4), 515–523. https://doi.org/10.1007/s11001-018-9354-7

Kunze, E., Firing, E., Hummon, J. M., Chereskin, T. K., & Thurnherr, A. M. (2006). Global abyssal mixing inferred from lowered ADCP shear and CTD strain profiles. *Journal of Physical Oceanography*, *36*(8), 1553–1576. https://doi.org/10.1175/JPO2926.1

Kunze, E., MacKay, C., McPhee-Shaw, E. E., Morrice, K., Girton, J. B., & Terker, S. R. (2012). Turbulent mixing and exchange with interior waters on sloping boundaries. *Journal of Physical Oceanography*, *42*(6), 910–927. https://doi.org/10.1175/jpo-d-11-075.1

Kunze, E., & Toole, J. M. (1997). Tidally driven vorticity, diurnal shear, and turbulence atop Fieberling Seamount. *Journal of Physical Oceanography*, *27*(12), 2663–2693. https://doi.org/10.1175/1520-0485(1997)027<2663:TDVDSA>2.0.CO;2

Ledwell, J., Montgomery, E., Polzin, K., Laurent, L. S., Schmitt, R., & Toole, J. (2000). Evidence for enhanced mixing over rough topography in the abyssal ocean. *Nature*, *403*(6766), 179–182. https://doi.org/10.1038/35003164

Locarnini, R. A., Mishonov, A. V., Antonov, J. I., Boyer, T. P., Garcia, H. E., Baranova, O. K. et al. (2013). World ocean atlas 2013, volume 1: Temperature.

Lueck, R. G., & Mudge, T. D. (1997). Topographically induced mixing around a shallow seamount. *Science*, *276*(5320), 1831–1833. https://doi.org/10.1126/science.276.5320.183

Lumpkin, R., & Speer, K. (2007). Global ocean meridional overturning. *Journal of Physical Oceanography*, *37*(10), 2550–2562. https://doi.org/10.1175/jpo3130.1

Ma, W., Wang, J., Wang, F., Zhang, Z., & Ma, Q. (2023). The vertical structure and intraseasonal variability of the deep currents in the Southern Philippine Basin. *Deep Sea Research Part I: Oceanographic Research Papers*, *197*, 104043. https://doi.org/10.1016/j.dsr.2023.104043

Mackinnon, J. A., Johnston, T. M. S., & Pinkel, R. (2008). Strong transport and mixing of deep water through the Southwest Indian Ridge. *Nature Geoscience*, *1*(11), 755–758. https://doi.org/10.1038/ngeo340

Marshall, J., & Speer, K. (2012). Closure of the meridional overturning circulation through Southern Ocean upwelling. *Nature Geoscience*, *5*(3), 171–180. https://doi.org/10.1038/ngeo1391

McDougall, T. J. (1984). The relative roles of diapycnal and isopycnal mixing on subsurface water mass conversion. *Journal of Physical Oceanography*, *14*(10), 1577–1589. https://doi.org/10.1175/1520-0485(1984)014<1577:TRRODA>2.0.CO;2

Munk, W. (1966). Abyssal recipes. *Deep-Sea Research and Oceanographic Abstracts*, *13*(4), 707–730. https://doi.org/10.1016/0011-7471(66)90602-4

Munk, W., & Wunsch, C. (1998). Abyssal recipes II: Energetics of tidal and wind mixing. *Deep Sea Research Part I: Oceanographic Research Papers*, *45*(12), 1977–2010. https://doi.org/10.1016/S0967-0637(98)00070-3

Nash, J. D., Kunze, E., Lee, C. M., & Sanford, T. B. (2006). Structure of the baroclinic tide generated at Kaena Ridge, Hawaii. *Journal of Physical Oceanography*, *36*(6), 1123–1135. https://doi.org/10.1175/JPO2883.1

Nikurashin, M., & Ferrari, R. (2011). Global energy conversion rate from geostrophic flows into internal lee waves in the deep ocean. *Geophysical Research Letters*, *38*(8), L08610. https://doi.org/10.1029/2011gl046576

Osborn, T. (1980). Estimates of the local rate of vertical diffusion from dissipation measurements. *Journal of Physical Oceanography*, *10*(1), 83–89. https://doi.org/10.1175/1520-0485(1980)010<0083:EOTLRO>2.0.CO;2

Polzin, K., Speer, K., Toole, J., & Schmitt, R. (1996). Intense mixing of Antarctic bottom water in the equatorial Atlantic Ocean. *Nature*, *380*(6569), 54–57. https://doi.org/10.1038/380054a0

Polzin, K., Toole, J., Ledwell, J., & Schmitt, R. (1997). Spatial variability of turbulent mixing in the abyssal ocean. *Science*, *276*(5309), 93–96. https://doi.org/10.1126/science.276.5309.93

Sen Gupta, A., McGregor, S., Van Sebille, E., Ganachaud, A., Brown, J. N., & Santoso, A. (2016). Future changes to the Indonesian Throughflow and Pacific circulation: The differing role of wind and deep circulation changes. *Geophysical Research Letters*, *43*(4), 1669–1678. https://doi.org/10.1002/2016GL067757

Siedler, G., Holfort, J., Zenk, W., Müller, T. J., & Csernok, T. (2004). Deep-water flow in the Mariana and Caroline Basins. *Journal of Physical Oceanography*, *34*(3), 566–581. https://doi.org/10.1175/2511.1

Sloyan, B. M. (2006). Antarctic bottom and lower circumpolar deep water circulation in the eastern Indian Ocean. *Journal of Geophysical Research*, *111*(C2), C02006. https://doi.org/10.1029/2005jc003011

St. Laurent, L. C., & Nash, J. D. (2004). An examination of the radiative and dissipative properties of deep ocean internal tides. *Deep Sea Research Part II: Topical Studies in Oceanography*, *51*(25–26), 3029–3042. https://doi.org/10.1016/j.dsr2.2004.09.008

St. Laurent, L. C., Toole, J. M., & Schmitt, R. W. (2001). Buoyancy forcing by turbulence above rough topography in the abyssal Brazil Basin. *Journal of Physical Oceanography*, *31*(12), 3476–3495. https://doi.org/10.1175/1520-0485(2001)031<3476:BFBTAR>2.0.CO;2

Talley, L. D. (2013). Closure of the global overturning circulation through the Indian, pacific, and southern oceans: Schematics and transports. *Oceanography*, *26*(1), 80–97. https://doi.org/10.5670/oceanog.2013.07

Talley, L. D., Pickard, G. L., Emery, W. J., & Swift, J. H. (2011). Arctic Ocean and Nordic Seas. *Descriptive Physical Oceanography*, 401–436. https://doi.org/10.1016/B978-0-7506-4552-2.10012-5

Thorpe, S. A. (1977). Turbulence and mixing in a Scottish loch. *Philosophical Transactions of the Royal Society of London - Series A: Mathematical and Physical Sciences*, *286*(1334), 125–181. https://doi.org/10.1098/rsta.1977.0112

Thurnherr, A. M., Clément, L., Laurent, L. S., Ferrari, R., & Ijichi, T. (2019). Transformation and upwelling of bottom water in fracture zone valleys. *Journal of Physical Oceanography*, *50*(3), 715–726. https://doi.org/10.1175/jpo-d-19-0021.1

Thurnherr, A. M., Laurent, L. S., Speer, K., Toole, J. M., & Ledwell, J. R. (2005). Mixing associated with sills in a canyon on the midocean ridge flank. *Journal of Physical Oceanography*, *35*(8), 1370–1381. https://doi.org/10.1175/JPO2773.1

Tian, J., Yang, Q., & Zhao, W. (2009). Enhanced diapycnal mixing in the South China Sea. *Journal of Physical Oceanography*, *39*(12), 3191–3203. https://doi.org/10.1175/2009jpo3899.1

Tian, Z., Zhou, C., Xiao, X., Wang, T., Qu, T., Yang, Q., et al. (2021). Water-mass properties and circulation in the deep and abyssal Philippine Sea. *Journal of Geophysical Research: Oceans*, *126*(6), e2020JC016994. https://doi.org/10.1029/2020jc016994

Toole, J. M., Schmitt, R. W., & Polzin, K. L. (1994). Estimates of diapycnal mixing in the abyssal ocean. *Science*, *264*(5162), 1120–1123. https://doi.org/10.1126/science.264.5162.1120

Tozer, B., Sandwell, D. T., Smith, W. H. F., Olson, C., Beale, J. R., & Wessel, P. (2019). Global bathymetry and topography at 15 arc sec: SRTM15+. *Earth and Space Science*, *6*(10), 1847–1864. https://doi.org/10.1029/2019ea000658

Uehara, K., & Taira, K. (1990). Deep hydrographic structure along 12°N and 13°N in the Philippine Sea. *Journal of the Oceanographical Society of Japan*, *46*(4), 167–176. https://doi.org/10.1007/BF02125577

Vic, C., Naveira Garabato, A. C., Green, J. A. M., Spingys, C., Forryan, A., Zhao, Z., & Sharples, J. (2018). The lifecycle of semidiurnal internal tides over the northern Mid-Atlantic Ridge. *Journal of Physical Oceanography*, *48*(1), 61–80. https://doi.org/10.1175/jpo-d-17-0121.1

Vic, C., Naveira Garabato, A. C., Green, J. A. M., Waterhouse, A. F., Zhao, Z., Melet, A., et al. (2019). Deep-ocean mixing driven by small-scale internal tides. *Nature Communications*, *10*(1), 2099. https://doi.org/10.1038/s41467-019-10149-5

Voet, G., Alford, M. H., MacKinnon, J. A., & Nash, J. D. (2020). Topographic form drag on tides and low-frequency flow: Observations of nonlinear lee waves over a tall submarine ridge near Palau. *Journal of Physical Oceanography*, *50*(5), 1489–1507. https://doi.org/10.1175/jpo-d-19-0257.1

Voet, G., Girton, J. B., Alford, M. H., Carter, G. S., Klymak, J. M., & Mickett, J. B. (2015). Pathways, volume transport, and mixing of abyssal water in the Samoan Passage. *Journal of Physical Oceanography*, *45*(2), 562–588. https://doi.org/10.1175/jpo-d-14-0096.1

Wang, J., Wang, F., Lu, Y., Ma, Q., Pratt, L. J., & Zhang, Z. (2021a). Pathways, volume transport, and seasonal variability of the lower deep limb of the Pacific Meridional Overturning Circulation at the Yap-Mariana Junction. *Frontiers in Marine Science*, *8*, 672199. https://doi.org/10.3389/fmars.2021.672199

Wang, J., Wang, F., Lu, Y., Zhang, H., Ma, Q., Pratt, L. J., & Zhang, Z. (2023). Abyssal circulation from the Yap-Mariana Junction to the Northern Philippine Basin. *Geophysical Research Letters*, *50*(6), e2022GL100610. https://doi.org/10.1029/2022gl100610

Wang, Y., Xu, Z., Hibiya, T., Yin, B., & Wang, F. (2021b). Radiation path of diurnal internal tides in the northwestern Pacific controlled by refraction and interference. *Journal of Geophysical Research: Oceans*, *126*(11), e2020JC016972. https://doi.org/10.1029/2020JC016972

Wang, Y., Xu, Z., Yin, B., Hou, Y., & Chang, H. (2018). Long-range radiation and interference pattern of multisource M2 internal tides in the Philippine Sea. *Journal of Geophysical Research: Oceans*, *123*(8), 5091–5112. https://doi.org/10.1029/2018jc013910

Xu, Z., Wang, Y., Liu, Z., McWilliams, J. C., & Gan, J. (2021). Insight into the dynamics of the radiating internal tide associated with the Kuroshio Current. *Journal of Geophysical Research: Oceans*, *126*(6), e2020JC017018. https://doi.org/10.1029/2020jc017018

Ye, R., Shang, X., Zhao, W., Zhou, C., Yang, Q., Tian, Z., et al. (2022). Circulation driven by multihump turbulent mixing over a seamount in the South China Sea. *Frontiers in Marine Science*, *8*, 794156. https://doi.org/10.3389/fmars.2021.794156

Yoshioka, N., Endoh, M., & Ishizaki, H. (1988). Observation of the abyssal current in the West Mariana Basin. *Journal of the Oceanographical Society of Japan*, *44*(1), 33–39. https://doi.org/10.1007/BF02303148

Zhai, F., & Gu, Y. (2020). Abyssal circulation in the Philippine Sea. *Journal of Ocean University of China*, *19*(2), 249–262. https://doi.org/10.1007/s11802-020-4241-7

Zhai, F., Wang, Q., Dunxin, H. U., & Guo, X. (2014). Observation of the abyssal western boundary current in the Philippine Sea. *Chinese Journal of Oceanology and Limnology*, *32*(5), 1188–1197. https://doi.org/10.1007/s00343-014-3339-4

Zhao, C., Xu, Z., Robertson, R., Li, Q., Wang, Y., & Yin, B. (2021). The three-dimensional internal tide radiation and dissipation in the Mariana Arc-Trench system. *Journal of Geophysical Research: Oceans*, *126*(5), e2020JC016502. https://doi.org/10.1029/2020jc016502

Zhao, Z., Alford, M. H., Girton, J. B., Rainville, L., & Simmons, H. L. (2016). Global observations of open-ocean Mode-1 M2 internal tides. *Journal of Physical Oceanography*, *46*(6), 1657–1684. https://doi.org/10.1175/jpo-d-15-0105.1

Zhou, C., Xu, H., Xiao, X., Zhao, W., Yang, J., Yang, Q., et al. (2022). Intense abyssal flow through the Yap-Mariana Junction in the Western North Pacific. *Geophysical Research Letters*, *49*(3), e2021GL096530. https://doi.org/10.1029/2021gl096530

Zhou, C., Zhao, W., Tian, J., Yang, Q., Huang, X., Zhang, Z., & Qu, T. (2018). Observations of deep current at the western boundary of the Northern Philippine Basin. *Scientific Reports*, *8*(1), 14334. https://doi.org/10.1038/s41598-018-32541-9

Zweng, M. M., Reagan, J. R., Antonov, J. I., Locarnini, R. A., Mishonov, A. V., Boyer, T. P., et al. (2013). World ocean atlas 2013, volume 2: Salinity.

References From the Supporting Information

MacKinnon, J., & Gregg, M. (2003). Mixing on the late-summer New England shelf—Solibores, shear, and stratification. *Journal of Physical Oceanography*, *33*(7), 1476–1492. https://doi.org/10.1175/1520-0485(2003)033<1476:MOTLNE>2.0.CO;2